


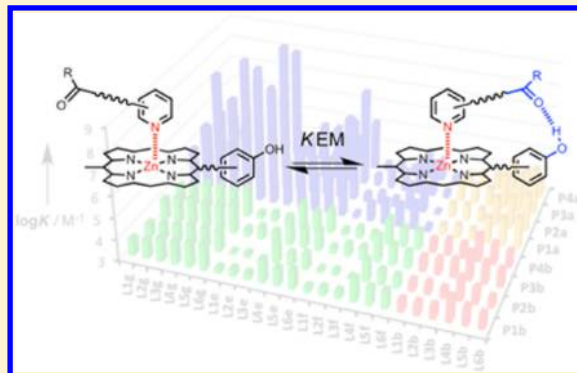
Relationship between Chemical Structure and Supramolecular Effective Molarity for Formation of Intramolecular H-Bonds

Hongmei Sun, Christopher A. Hunter,* Cristina Navarro, and Simon Turega

Department of Chemistry, University of Sheffield, Sheffield S3 7HF, U.K.

 Supporting Information

ABSTRACT: Effective molarity (EM) is a key parameter that determines the efficiency of a range of supramolecular phenomena from the folding of macromolecules to multivalent ligand binding. Coordination complexes formed between zinc porphyrins equipped with H-bond donor sites and pyridine ligands equipped with H-bond acceptor sites have allowed systematic quantification of EM values for the formation of intramolecular H-bonds in 240 different systems. The results provide insights into the relationship of EM to supramolecular architecture, H-bond strength, and solvent. Previous studies on ligands equipped with phosphonate diester and ether H-bond acceptors were inconclusive, but the experiments described here on ligands equipped with phosphine oxide, amide, and ester H-bond acceptors resolve these ambiguities. Chemical double-mutant cycles were used to dissect the thermodynamic contributions of individual H-bond interactions to the overall stabilities of the complexes and hence determine the values of EM, which fall in the range 1–1000 mM. Solvent has little effect on EM, and the values measured in toluene and 1,1,2,2-tetrachloroethane are similar. For H-bond acceptors that have similar geometries but different H-bond strengths (amide and ester), the values of EM are very similar. For H-bond acceptors that have different geometries but similar H-bond strengths (amide and phosphonate diester), there is little correlation between the values of EM. These results imply that supramolecular EMs are independent of solvent and intrinsic H-bond strength but depend on supramolecular architecture and geometric complementarity.



INTRODUCTION

Molecular recognition and self-assembly processes depend on the interplay of multiple intermolecular interactions. Cooperativity between different non-covalent interaction sites in a complex interface can have dramatic effects on the overall binding affinities of the components. This phenomenon has been extensively exploited in the design of high-affinity synthetic receptors for ions and in the development of multivalent ligands for biological receptors.^{1–7} However, understanding the relationship between chemical structure and the magnitude of cooperative effects remains an important challenge that must be overcome if we are to develop reliable strategies for the design of new supramolecular systems with predictable properties.

Cooperativity can take the form of allosteric interactions that alter the intrinsic binding properties at different interaction sites, as in hemoglobin, or chelate cooperativity that leads to an enhanced binding affinity in systems that feature multiple intermolecular interactions.^{8,9} Chelate cooperativity leads to many of the all-or-nothing processes that are characteristic features of biological systems that switch between different states over a narrow range of conditions.^{10–13} Chelate cooperativity is also central to the design of high-affinity molecular recognition systems and efficient self-assembly processes.^{14,15} Although we have a qualitative understanding

of this phenomenon (geometric complementarity and preorganization lead to high affinity), quantification of the magnitudes of these effects has proved more elusive.^{16–20} Perfect geometric complementarity and conformational rigidity are usually difficult to achieve, so it would be useful to have quantitative guidelines for estimating the penalties for imperfect design and the potential benefits that would accrue from synthetically more challenging targets. In this paper, we describe experiments designed to quantify the relationship between chemical structure and chelate cooperativity using a synthetic model system.

The parameter used to quantify chelate cooperativity is effective molarity (EM), which is defined as the ratio of the intramolecular association constant for an interaction to the corresponding intermolecular association constant for the same interaction in a reference system.^{21–23} This is a thermodynamic effective molarity; it is also possible to define a kinetic effective molarity in the same way by using rate constants in place of equilibrium constants. A large body of experimental data on EM for intramolecular covalent bond formation has been collected, and values as high as 10¹⁴ M have been reported.²² Increasing the conformational flexibility of the chain linking the

Received: June 22, 2013

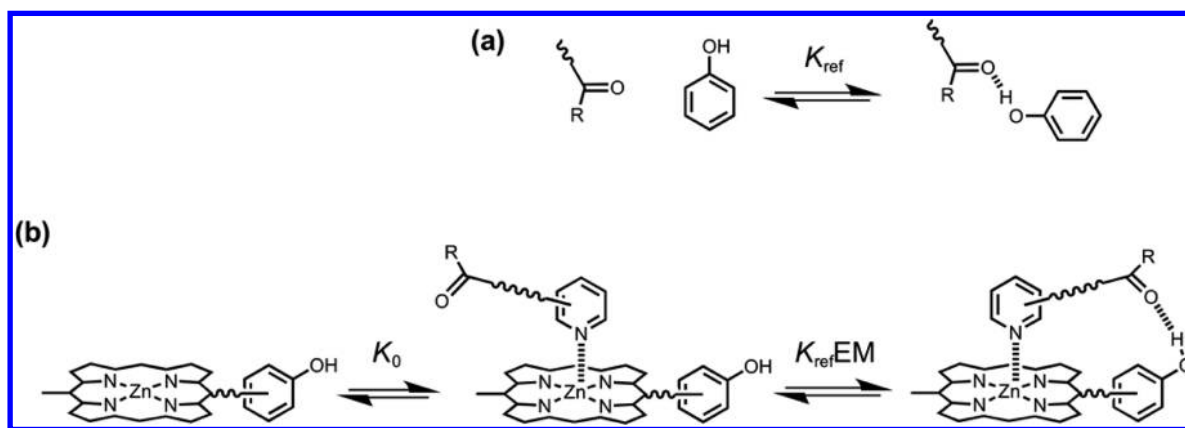


Figure 1. (a) Formation of an intermolecular H-bond. (b) Stepwise equilibria in the formation of a porphyrin–pyridine complex containing an intramolecular H-bond. K_{ref} is the equilibrium constant for formation of the intermolecular H-bond. K_0 is the intermolecular association constant for formation of the zinc–nitrogen interaction. $K_{\text{ref}}EM$ is the equilibrium constant for formation of the intramolecular H-bond, and EM is the effective molarity for the intramolecular interaction.

two reaction sites and decreasing the geometric complementarity of the linker can reduce the value of EM by many orders of magnitude.^{24,25} The experimental data that are available on EM for intramolecular non-covalent bond formation suggest that supramolecular EMs are quite different from covalent EMs. The values of non-covalent EMs do not exceed 10^3 M and are subject to less dramatic variation than covalent EMs.²⁶ We have begun a systematic study using porphyrin–pyridine complexes to quantify the variation in supramolecular EM with geometric complementarity, conformational flexibility, intrinsic functional group interaction strength, and solvent.^{27–34} The results that we have reported to date show conflicting trends, so in this paper, we significantly expand the number of different systems studied and compare measurements of intramolecular H-bonding interactions in 240 different complexes.

Approach. We previously developed the porphyrin–ligand system shown in Figure 1b for the quantification of chelate cooperativity in complexes that make multiple intermolecular interactions.²⁷ The pyridine–zinc coordination interaction in Figure 1b gives a complex in which the formation of an intramolecular H-bond between the porphyrin phenol groups and H-bond acceptors on the ligand is possible. Strictly, this H-bond is a second intermolecular interaction, but in the stepwise pathway shown in Figure 1b, the H-bond is an intracomplex interaction, so we will refer to this as an intramolecular interaction. The double-mutant cycle (DMC) shown in Figure 2 dissects out the thermodynamic contribution of the

intramolecular acceptor–donor (A·D) H-bond to the overall stability of complex A.^{35,36} The DMC works by removing the thermodynamic contributions due to the secondary interactions that are highlighted in Figure 2. For example, secondary interactions associated with mutation of the ligand from LA to L contribute to the difference between the stabilities of complexes A and B and to the difference between the stabilities of complexes C and D. Similarly, secondary interactions associated with mutating the porphyrin from PD to P contribute to the difference between the stabilities of complexes A and C and to the difference between the stabilities of complexes B and D. In eq 1, these differences cancel out, providing a direct measurement of the free energy contribution due to the A·D H-bond in complex A ($\Delta\Delta G^\circ$):

$$\Delta\Delta G^\circ = \Delta G_A^\circ - \Delta G_B^\circ - \Delta G_C^\circ + \Delta G_D^\circ \quad (1)$$

The EM for the intramolecular interaction can be determined by comparing the intramolecular interaction with the corresponding intermolecular interaction measured in a reference system (Figure 1a). Figure 1b shows that the equilibrium constant for formation of an intramolecular H-bond can be expressed as $K_{\text{ref}}EM$, where K_{ref} is the equilibrium constant for the intermolecular process illustrated in Figure 1a. This separates the thermodynamic properties of the intramolecular interaction into K_{ref} , which is related to the intrinsic properties of the functional group interaction, and EM, which measures the influence of the supramolecular architecture on chelate cooperativity.

In previous work, we investigated chelate cooperativity using pyridine ligands equipped with either phosphonate diester or ether H-bond acceptors in two different solvents, toluene and 1,1,2,2-tetrachloroethane (TCE).^{27,28,31,32} In TCE, the two different types of H-bond have similar values of EM when they are mounted on the same supramolecular framework.³² The values of EM were similar in toluene and TCE for the ether ligands, but for the phosphonate diester ligands, the values of EM in toluene were significantly higher than those in TCE.^{31,32} The phenol–ether H-bond is much weaker than the phenol–phosphonate diester H-bond, so the number of ether ligands for which it was possible to measure the value of EM was relatively small. There are also some differences between the geometries and steric properties of the ether and phosphonate diester ligands (Figure 3a), which could account for the

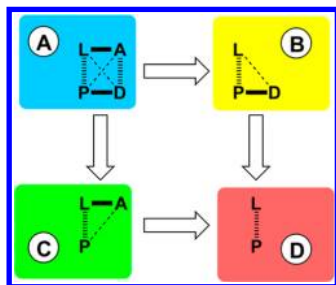


Figure 2. Chemical double-mutant cycle (DMC) for measurement of the free energy contribution of the A·D H-bond to the stability of complex A. P is a zinc porphyrin, PD is a zinc porphyrin equipped with a H-bond donor (D), L is a pyridine ligand, and LA is a pyridine ligand equipped with a H-bond acceptor (A).

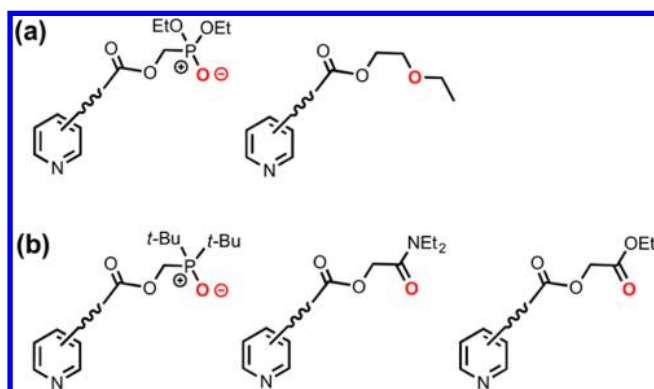


Figure 3. Pyridine ligands having an oxygen H-bond acceptor atom (red) located at the same point on the ligand framework: (a) previously reported phosphonate diester and ether ligands; (b) phosphine oxide, amide, and ester ligands reported in this paper.

difference in behavior. In the present work, we expanded the range of ligand systems to include phosphine oxide, amide, and ester H-bond acceptor ligands (Figure 3b) to provide a more comprehensive data set of supramolecular EMs. The five ligand systems illustrated in Figure 3 all have a H-bond acceptor oxygen atom (highlighted in red) located at the same point on the ligand framework. Comparison of the values of EM measured for a range of different functional groups mounted on the same ligand framework provides a good test of whether the EM for an intramolecular H-bond is influenced by the intrinsic properties of the functional group interaction, the overall stability of the complex, or the solvent or is simply a function of the supramolecular architecture.

RESULTS AND DISCUSSION

The structures of the porphyrins and ligands used in this study are shown in Figures 4 and 5, respectively. **P1a–P4a** are zinc porphyrins equipped with peripheral H-bond donor sites at

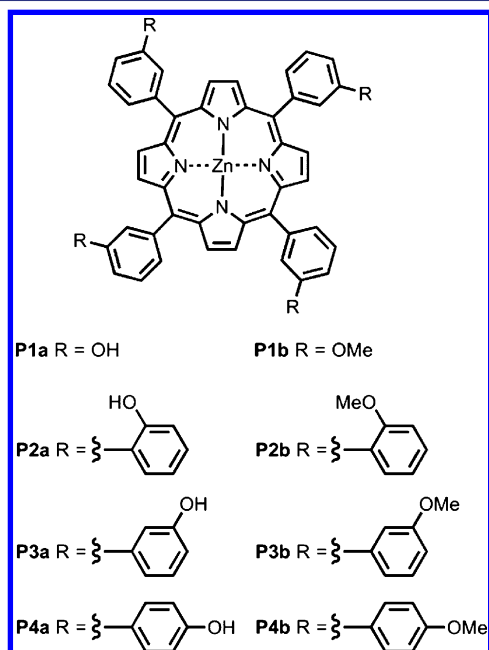


Figure 4. Porphyrin receptors **P1a–P4a** that can make H-bonds and **P1b–P4b** that cannot.

different positions, and **P1b–P4b** are the corresponding methoxy-substituted porphyrins used as the non-H-bonding mutants in the DMCs. The synthesis of the porphyrins was reported previously.²⁷ The syntheses of the ligands featuring phosphonate diester or ether H-bond acceptors (**La** and **Ld**) and the non-H-bonding mutants (**Lb** and **Lc**) have been described in previous publications.^{27,28}

Syntheses. The ligands equipped with tertiary amide, ester, and phosphine oxide H-bond acceptor sites (**Le**, **Lf**, and **Lg**) were prepared from the corresponding pyridinecarboxylic acids via the acid chlorides (Scheme 1). Two of the alcohols used in the acid chloride couplings are commercially available, *N,N*-diethyl-2-hydroxyacetamide and ethyl glycolate. Alcohol **1** required for the phosphine oxide ligands was prepared in one step from di-*tert*-butylchlorophosphine and formaldehyde (Scheme 2a).

Phosphine oxide **2** was synthesized in order to measure the H-bonding properties of this functional group, in particular the value of K_{ref} for use in determining the EM for intramolecular phosphine oxide–phenol H-bonds. Scheme 2b shows the synthetic route, which gave **2** in low yield but in sufficient quantities for use in ¹H NMR titrations.³⁷

An additional ligand **Q** equipped with a pyromellitimide electron acceptor moiety was synthesized for use in competition titrations to characterize very high affinity complexes (Scheme 3). Condensation of pyromellitic anhydride with *n*-hexylamine and 3-(aminomethyl)pyridine gave a mixture of products, which were separated by column chromatography to obtain the required unsymmetrical pyromellitimide ligand **Q**.³⁸

Measurement of Porphyrin–Ligand Binding Interactions. Binding of the ligands to the porphyrins was studied in toluene and in TCE using titrations monitored by UV/vis absorption spectroscopy. There were 144 different porphyrin–ligand combinations, but for association constants lower than 10^6 M^{-1} , the titration experiments could be automated using a UV/vis plate reader.²⁷ Binding of pyridine to a zinc porphyrin leads to a large change in the Soret absorption band, and a well-defined isosbestic point indicates the formation of a 1:1 complex. The UV/vis absorption titration data fit well to a 1:1 binding isotherm, and the results are reported in the Supporting Information.

Some porphyrin–ligand combinations gave exceptionally stable complexes, particularly the phosphine oxide ligands in toluene, where the H-bonding interactions are strongest. For these systems, fluorescence titrations were required in order to measure the association constants. A plate reader equipped with fluorescence detection allowed automated measurement of association constants in the range 10^6 to 10^7 M^{-1} . A more sensitive fluorimeter was used to measure association constants in the range 10^7 to 10^8 M^{-1} by manual titrations. In all cases, the titration data fit well to a 1:1 binding isotherm. However for some of the complexes, the association constants were too high for reliable measurement by these methods, and a competition experiment was therefore developed. When ligand **Q** equipped with a pyromellitimide moiety, which is a good electron acceptor, was added to any of the zinc porphyrins, the porphyrin fluorescence was quenched by photoinduced electron transfer from the porphyrin excited state to the pyromellitimide (Figure 6a).³⁸ Subsequent addition of a different ligand that binds more strongly to the porphyrin displaced **Q** and restored the porphyrin fluorescence (Figure 6b). This system provided a convenient competition binding

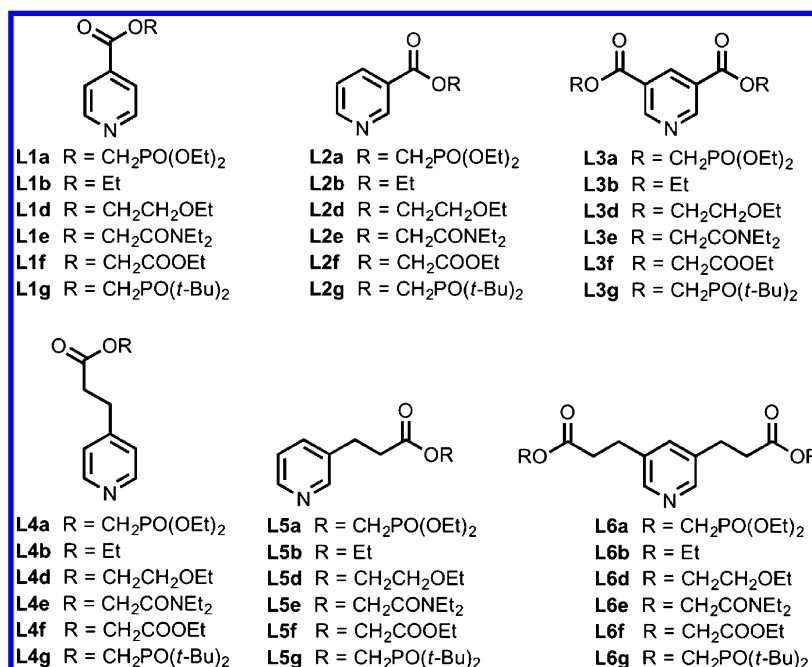
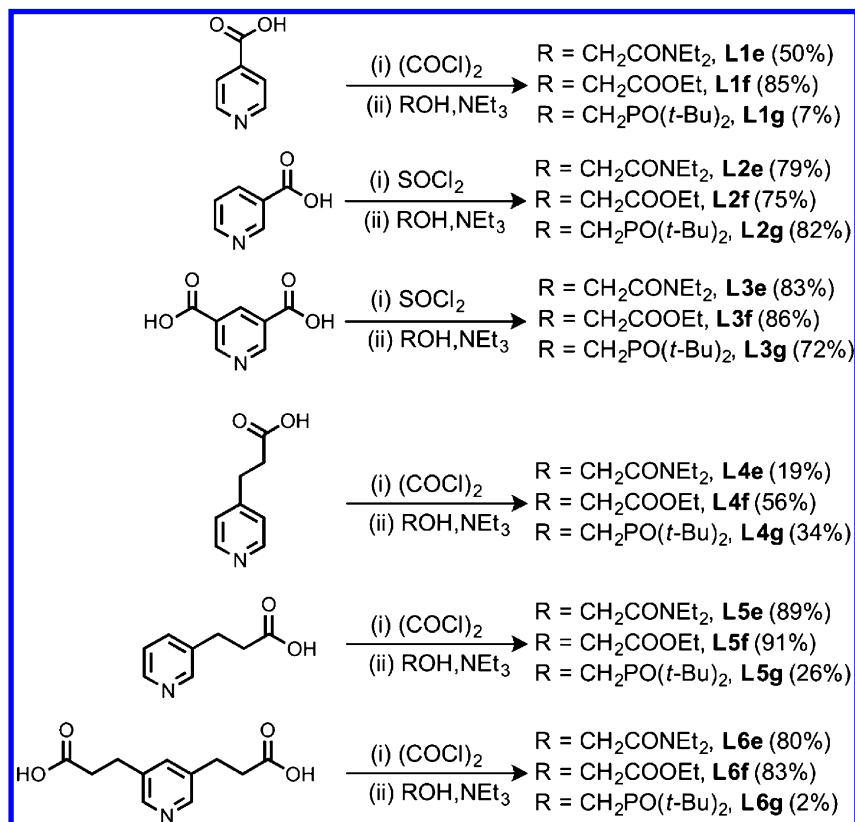


Figure 5. Pyridine ligands.

Scheme 1



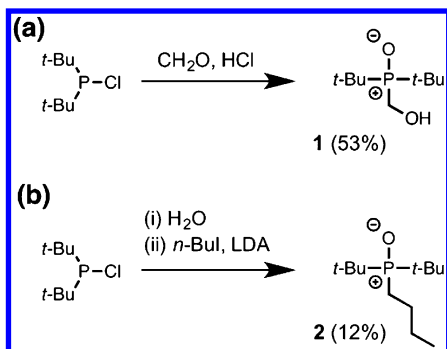
assay that could be monitored by fluorescence, allowing accurate measurement of very high association constants.

The titration data for the ligand displacement experiments could be fit to a simple 1:1 binding isotherm provided that **Q** was present in a large excess relative to the porphyrin and that the total concentration of **Q** was constant throughout the titration. Under these conditions, the apparent value of the

association constant obtained by fitting the data to a 1:1 binding isotherm, K_{app} , is related to the true association constant for formation of the porphyrin–ligand complex, K_L , by eq 2:

$$K_{app} = \frac{K_L}{1 + K_Q[Q]} \quad (2)$$

Scheme 2



where K_Q is the association constant for the formation of the porphyrin-**Q** complex and $[Q]$ is the total concentration of **Q** (see the Experimental Section for details). Thus, the ligand solution added to the porphyrin solution during the titration had to contain the same concentration of **Q** as present in the porphyrin solution.

Figure 7 compares fluorescence titration data collected under these conditions with the corresponding UV/vis absorption data for the titration of **L6g** with **P3a**. The association constant for this complex is $K_L = 8 \times 10^8 \text{ M}^{-1}$, and the UV/vis absorption data could not be used to determine the association constant because the tight binding limit was reached under the conditions of the experiment (Figure 7a). Addition of 10 mM **Q** reduced K_{app} to $4 \times 10^6 \text{ M}^{-1}$, allowing straightforward determination of K_L by the fluorescence displacement experiment (Figure 7b). Equation 2 shows that varying the concentration of **Q** enables K_{app} to be adjusted to a conveniently measurable value, allowing experiments to be carried out in different concentration regimes for different complexes, which makes this a particularly versatile technique.

The association constants for these complexes span 8 orders of magnitude, ranging from 10^1 to 10^9 M^{-1} depending on the H-bonding functionality, solvent, and porphyrin–ligand complementarity. Figure 8 shows the relationship between the association constants measured in TCE and the corresponding values measured in toluene. There is a reasonable correlation between the results obtained in the two solvents. In all cases, the association constants are 1–2 orders of magnitude bigger in toluene than in TCE, which is more polar and competes with both the zinc–nitrogen coordination and intramolecular H-bonding interactions. Dissection of the relative contributions of the coordination bond and H-bonds to the overall association constant requires the DMC analysis illustrated in Figure 2.

DMC Analysis. The association constants are illustrated graphically in Figure 9. The complexes are organized and colored according to their role in the DMC in Figure 2. In general, the LA·PD complexes, where intramolecular H-bonding is possible, are more stable than the reference complexes LA·P, L·PD, and L·P, where these H-bonds are

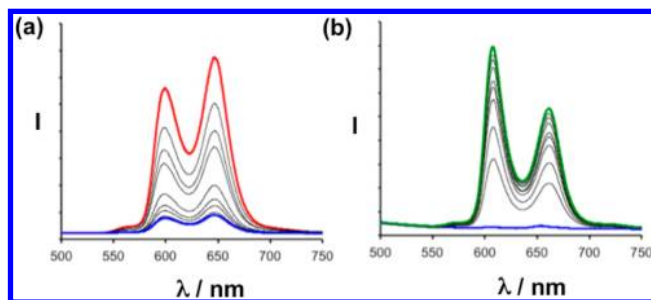


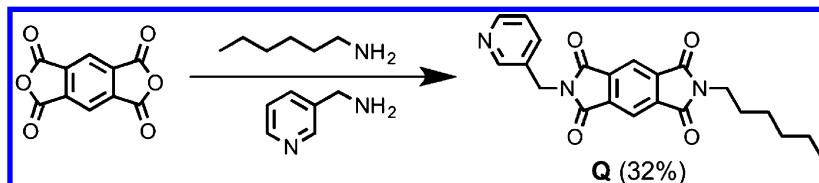
Figure 6. (a) Fluorescence spectra of **P3a** ($5 \mu\text{M}$) recorded during a titration with ligand **Q** in toluene at 298 K (red corresponds to free **P3a** and blue to the end point of the titration). (b) Fluorescence spectra recorded during a titration of **L6g** into a solution containing $0.4 \mu\text{M}$ **P3a** and 10 mM **Q** in toluene at 298 K (blue corresponds to the **P3a·Q** complex and green to the **P3a·L6g** complex). The fluorescence emission intensity (I) is plotted in arbitrary units, and the excitation wavelength was 427 nm in both cases.

absent. Among the LA·PD complexes, the phosphine oxide ligand complexes are more stable than the amide ligand complexes, which in turn are more stable than the ester ligand complexes. This is consistent with the H-bond acceptor parameters for these functional groups ($\beta = 10.2$ for a phosphine oxide, $\beta = 8.5$ for an amide, and $\beta = 5.3$ for an ester).³⁹ The free energy contributions due to intramolecular H-bonding interactions, $\Delta\Delta G^\circ$, were determined using eq 1, and the results are presented in Tables 1–6.

Intramolecular H-bonds contribute up to 26 kJ mol^{-1} to the free energy or 4 orders of magnitude to the stability of the porphyrin–ligand complexes. In toluene, all 24 of the phosphine oxide ligand–porphyrin combinations formed detectable intramolecular H-bonds, but the variation in geometric complementarity in these systems led to large variations in the free energy contribution from these interactions. The values of $\Delta\Delta G^\circ$ for the amide ligand complexes were somewhat lower than those for the phosphine oxide ligand complexes, but 22 of the 24 porphyrin–amide ligand combinations formed detectable intramolecular H-bonds in toluene (20 out of 24 in TCE). In contrast, values of $\Delta\Delta G^\circ$ for the ester ligand complexes were much lower, and only three of the 24 different porphyrin–ester ligand combinations formed detectable intramolecular H-bonds. These results are consistent with the H-bond acceptor parameters for the three functional groups: phosphine oxides ($\beta = 10.2$) are more polar than amides ($\beta = 8.5$), which in turn are much more polar than esters ($\beta = 5.3$).³⁹ In general, the H-bonding interactions were stronger in toluene than in TCE, which reflects the relative polarity of the two solvents.

One assumption of the DMC approach is that the free energy contributions that different interactions make to the overall stability of a complex are additive, and the data in Tables 1–6 provide an opportunity to test the validity of this assumption.⁴⁰ The **L3** and **L6** ligands are symmetrical two-

Scheme 3



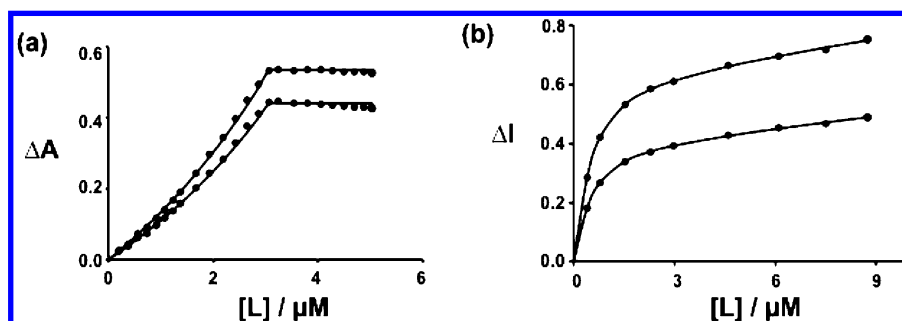


Figure 7. (a) Data recorded at two different wavelengths during an automated UV/vis absorption titration of **L6g** into **P3a** ($5 \mu\text{M}$) in toluene at 298 K. The lines correspond to best fits to a 1:1 binding isotherm with a linear correction for nonspecific effects (the curvature during the first phase of the titration is due to the increase in path length during a plate reader titration). (b) Data recorded at two different wavelengths during a fluorescence displacement experiment in which a solution containing $40 \mu\text{M}$ **L6g** and 10 mM **Q** was titrated into a solution containing $0.4 \mu\text{M}$ **P3a** and 10 mM **Q** in toluene at 298 K (excitation at 427 nm). The lines corresponds to best fits to a 1:1 binding isotherm with a linear correction for nonspecific effects.

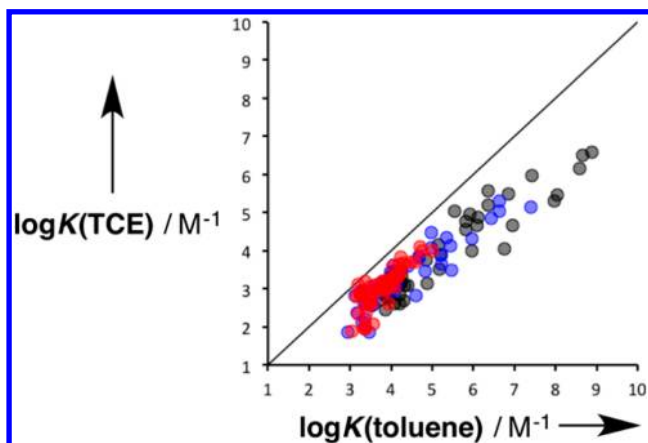


Figure 8. Comparison of association constants ($\log K/\text{M}^{-1}$) measured in toluene with the corresponding values measured in TCE. Data for phosphine oxide (**Lg**), amide (**Le**), and ester (**Lf**) ligands are shown in black, blue, and red, respectively. The line corresponds to $\log K(\text{TCE})/\text{M}^{-1} = \log K(\text{toluene})/\text{M}^{-1}$.

armed versions of the **L2** and **L5** ligands, respectively. If the free energy contributions from H-bonding in these complexes are additive, then the values of $\Delta\Delta G^\circ$ measured for the two-armed ligands should be double the values measured for the corresponding one-armed ligands. Figure 10 shows that this is indeed the case, confirming the additivity in these systems.

Pairwise differences in free energy between mutant complexes where the H-bonding functionality is missing, $\Delta G_B^\circ - \Delta G_D^\circ$ and $\Delta G_C^\circ - \Delta G_D^\circ$, provide information on the magnitude of secondary interactions in these systems. Figure 11a compares the values of $\Delta G_B^\circ - \Delta G_D^\circ$ measured in TCE with the corresponding values measured in toluene. For most of the systems, the values are close to zero, indicating that there are no significant secondary interactions. However, there are six systems where complex **B** is between -3 and -8 kJ mol^{-1} more stable than complex **D** in both solvents. This is clear evidence for attractive secondary interactions in complex **B**. We previously identified these secondary interactions as ester-phenol H-bonds involving the ligand linker group in the complexes of **L5b** and **L6b** with porphyrins **P1a**, **P2a**, and **P3a** (Figure 12).²⁷ The same interactions are present in complex **A** of the DMC, so the contribution from these secondary interactions cancels out in the DMC as shown in Figure 12,

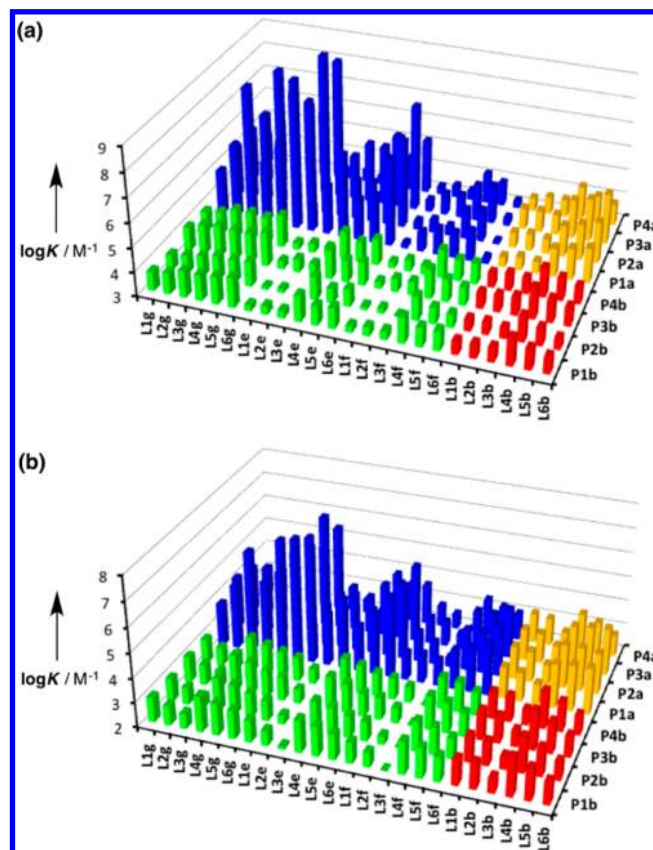


Figure 9. Association constants ($\log K/\text{M}^{-1}$) for formation of porphyrin–ligand complexes at 298 K in (a) toluene and (b) TCE. The data are color-coded according to the DMC in Figure 2: LA-PD (complex **A**) in blue, L-PD (complex **B**) in yellow, LA-P (complex **C**) in green, and L-P (complex **D**) in red.

and it is possible to obtain reliable values for intramolecular H-bonding interactions in the **L5** and **L6** ligand series.

Figure 11b compares values of $\Delta G_C^\circ - \Delta G_D^\circ$ measured in TCE with the corresponding values measured in toluene. Many of the systems give values close to zero, but there are two groups of data points that deviate significantly from zero. The ester (red) and amide (blue) ligands in the **L1**, **L2**, and **L3** ligand series give positive values of $\Delta G_C^\circ - \Delta G_D^\circ$ in TCE. This implies that there are secondary interactions with the H-bond acceptor functionality that destabilize complex **C**, and we

Table 1. Free Energy Contributions from Phosphine Oxide–Phenol H-Bonds ($\Delta\Delta G^\circ/\text{kJ mol}^{-1}$) Determined Using the DMC in Figure 2 at 298 K in Toluene^a

	L1g	L2g	L3g	L4g	L5g	L6g
P1a	−7	−13	−26	−8	−10	−21
P2a	−8	−7	−13	−9	−7	−12
P3a	−6	−9	−20	−13	−7	−18
P4a	−2	−5	−15	−10	−9	−20

^aOxygen–zinc coordination interactions in complexes **A** and **C** mean that these values underestimate the contribution of intramolecular H-bonds by up to 6 kJ mol^{−1}.

Table 2. Free Energy Contributions from Phosphine Oxide–Phenol H-Bonds ($\Delta\Delta G^\circ/\text{kJ mol}^{-1}$) Determined Using the DMC in Figure 2 at 298 K in TCE^a

	L1g	L2g	L3g	L4g	L5g	L6g
P1a	−3	−10	−19	−8	−9	−14
P2a	−5	−3	−7	−6	−6	−12
P3a	−4	−6	−14	−10	−7	−14
P4a	0	−2	−12	−8	−7	−13

^aOxygen–zinc coordination interactions in complexes **A** and **C** mean that these values underestimate the contribution of intramolecular H-bonds by up to 5 kJ mol^{−1}. Values of $\Delta\Delta G^\circ$ for complexes that do not make detectable H-bonds are set in italic type.

Table 3. Free Energy Contributions from Amide–Phenol H-Bonds ($\Delta\Delta G^\circ/\text{kJ mol}^{-1}$) Determined Using the DMC in Figure 2 at 298 K in Toluene^a

	L1e	L2e	L3e	L4e	L5e	L6e
P1a	−5	−10	−19	−3	−4	−11
P2a	−5	−4	−8	−3	−6	−10
P3a	−3	−6	−11	−5	−7	−12
P4a	−2	−1	0	−5	−2	−6

^aThe average error over the data set was ± 1 kJ mol^{−1}. Values of $\Delta\Delta G^\circ$ for complexes that do not make detectable H-bonds are set in italic type.

Table 4. Free Energy Contributions from Amide–Phenol H-Bonds ($\Delta\Delta G^\circ/\text{kJ mol}^{-1}$) Determined Using the DMC in Figure 2 at 298 K in TCE^a

	L1e	L2e	L3e	L4e	L5e	L6e
P1a	−2	−8	−14	−2	−4	−7
P2a	−3	−3	−4	−1	−4	−7
P3a	−2	−4	−8	−3	−3	−7
P4a	1	1	−1	−3	−2	−4

^aThe average error over the data set was ± 1 kJ mol^{−1}. Values of $\Delta\Delta G^\circ$ for complexes that do not make detectable H-bonds are set in italic type.

previously suggested that this could be due to adverse steric effects associated with solvation of the polar functional groups by the bulky solvent.³⁰ In contrast, the phosphine oxide ligands (black) give negative values of $\Delta G_C^\circ - \Delta G_D^\circ$ in toluene, indicating that there are secondary interactions that stabilize complex **C** in these systems. The NMR studies discussed below shed some light on the origin of this behavior.

Structural Information on Binding Modes. ¹H NMR spectra of 1:1 mixtures of porphyrins and ligands were recorded in toluene and in TCE. For some of the complexes in toluene, large upfield complexation-induced changes in ¹H NMR

Table 5. Free Energy Contributions from Ester–Phenol H-Bonds ($\Delta\Delta G^\circ/\text{kJ mol}^{-1}$) Determined Using the DMC in Figure 2 at 298 K in Toluene^a

	L1f	L2f	L3f	L4f	L5f	L6f
P1a	0	−3	−5	1	0	−1
P2a	0	−1	−1	0	1	0
P3a	0	−1	−2	0	1	0
P4a	−1	0	0	1	0	0

^aThe average error over the data set was ± 1 kJ mol^{−1}. Values of $\Delta\Delta G^\circ$ for complexes that do not make detectable H-bonds are set in italic type.

Table 6. Free Energy Contributions from Ester–Phenol H-Bonds ($\Delta\Delta G^\circ/\text{kJ mol}^{-1}$) Determined Using the DMC in Figure 2 at 298 K in TCE^a

	L1f	L2f	L3f	L4f	L5f	L6f
P1a	0	−3	−5	0	0	−1
P2a	0	−1	−1	0	0	−1
P3a	0	−1	−2	−1	1	0
P4a	1	1	0	−1	0	0

^aThe average error over the data set was ± 1 kJ mol^{−1}. Values of $\Delta\Delta G^\circ$ for complexes that do not make detectable H-bonds are set in italic type.

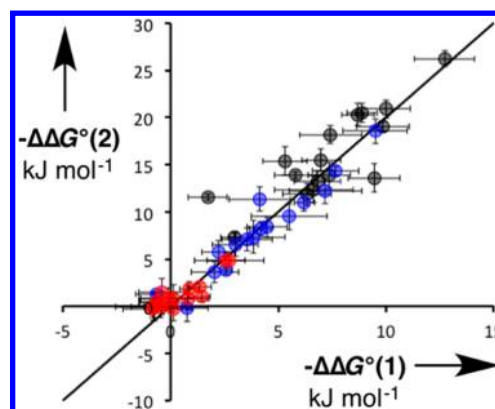


Figure 10. Total free energy contributions due to intramolecular H-bonding for ligands with two identical side arms, $\Delta\Delta G^\circ(2)$, compared with data for the corresponding one-armed ligands, $\Delta\Delta G^\circ(1)$. Data for phosphine oxide (Lg), amide (Le), and ester (Lf) ligands are shown in black, blue, and red, respectively. The line corresponds to $\Delta\Delta G^\circ(2) = 2\Delta\Delta G^\circ(1)$.

chemical shift were observed for the signal due to the phosphine oxide *tert*-butyl protons (see the Supporting Information). This implies that the phosphine oxide group sits over the center of the porphyrin ring current in these complexes, suggesting that the phosphine oxide oxygen may compete with the pyridine nitrogen for coordination to the zinc. To assess the extent of the problem, we titrated **P1b** into ligand **L2g**. Figure 13 shows the results of fitting the ¹H NMR titration data to a 2:1 binding isotherm. The limiting complexation-induced changes in chemical shift for formation of the 1:1 complex ($K_1 = 8 \times 10^3 \text{ M}^{-1}$) were −1.7 ppm for the *tert*-butyl signal and −0.5 ppm for the signal due to the pyridine α proton, and the subsequent changes in chemical shift for formation of the 2:1 complex ($K_2 = 7 \times 10^2 \text{ M}^{-1}$) were −0.7 ppm for the *tert*-butyl signal and −1.5 ppm for the signal due to the pyridine α proton. This suggests that the predominant binding mode in the **P1b**·**L2g** 1:1 complex is coordination of

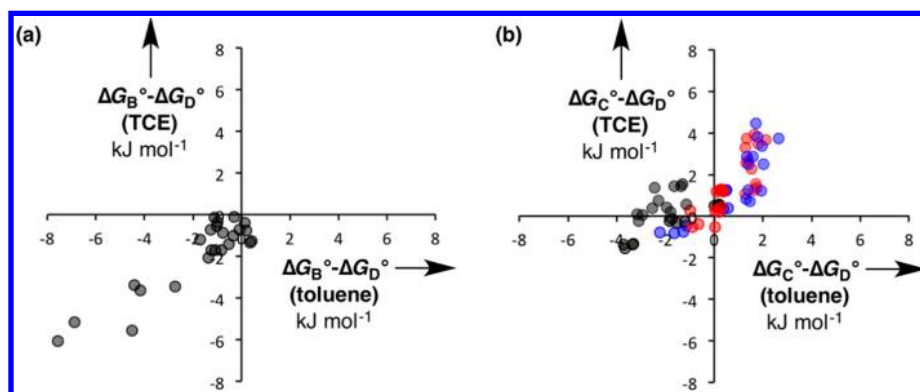


Figure 11. Secondary interactions measured in the DMCs. (a) Comparison of $\Delta G_B^\circ - \Delta G_D^\circ$ measured in TCE with corresponding values measured in toluene. (b) Comparison of $\Delta G_C^\circ - \Delta G_D^\circ$ measured in TCE with corresponding values measured in toluene. Data for phosphine oxide (**Lg**), amide (**Le**), and ester (**Lf**) ligands are shown in black, blue, and red, respectively.

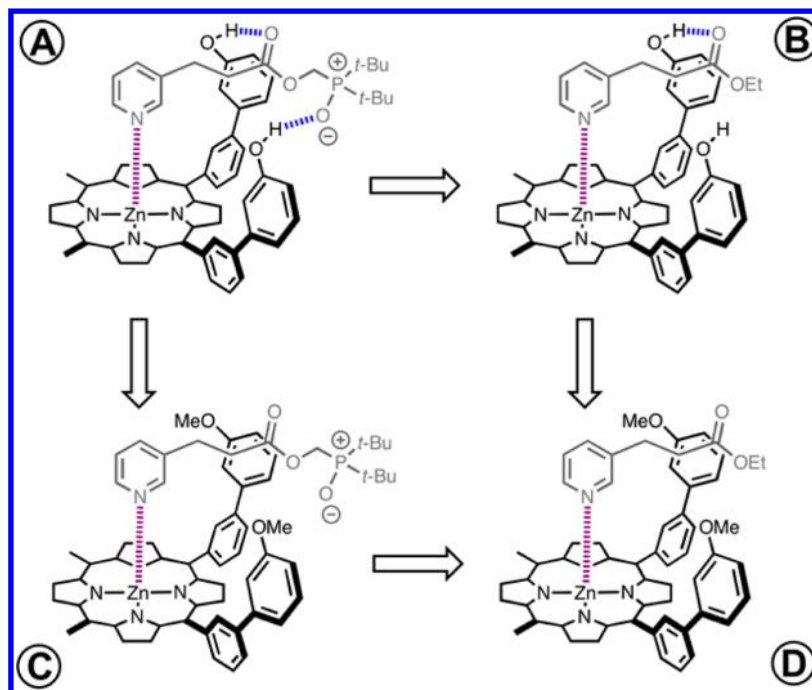


Figure 12. DMC used to measure the magnitude of the phosphine oxide–phenol H-bond in the **P3a·L5g** complex (complex A). The secondary ester–phenol H-bonding interactions, which are present in complexes **A** and **B** for ligand series **L5** and **L6**, give rise to large negative values of $\Delta G_B^\circ - \Delta G_D^\circ$ but cancel out in the DMC.

zinc by the phosphine oxide oxygen, and the second weaker binding event in the 2:1 complex is coordination of a second zinc porphyrin by the pyridine nitrogen. The values of K_1 and K_2 indicate that phosphine oxide coordination is about 10 times stronger than pyridine coordination, and this limits the accuracy of the DMC analysis for these systems. The values of $\Delta\Delta G^\circ$ measured by DMCs for the phosphine oxide ligands underestimate the free energy contributions due to intramolecular H-bonds by as much as 6 kJ mol^{−1} (see the Supporting Information).

Effective Molarities. The values of $\Delta\Delta G^\circ$ for intramolecular H-bonding can be converted into effective molarities (EM) using the corresponding association constants for formation of intermolecular H-bonds, K_{ref} . Figure 14 shows the structures of the compounds used to measure values of K_{ref} by ¹H NMR titrations with *p*-cresol in TCE and in toluene. The titration data fit well to a 1:1 binding isotherm, and the results

are shown in Table 7. It is also possible to estimate the value of K_{ref} using K_{calc} from eq 3,

$$-RT \ln K_{\text{calc}} = -(\alpha - \alpha_s)(\beta - \beta_s) + 6 \text{ kJ mol}^{-1} \quad (3)$$

where α and β are the H-bond parameters for the H-bond donor and acceptor and α_s and β_s are the H-bond parameters for the solvent. The agreement with the experimentally determined values is good (Table 7).³⁹

In a complex held together by multiple non-covalent interactions, the bound state is actually a mixture of partially and fully bound states.^{27,34} For example, the complex shown in Figure 1a is a mixture the partially bound state, where only the zinc–nitrogen bond is formed, and the fully bound state, where both the zinc–nitrogen bond and the intramolecular H-bond are formed. The association constant that is measured experimentally, K_{obs} , is the sum of the association constants of all bound states (eq 4).

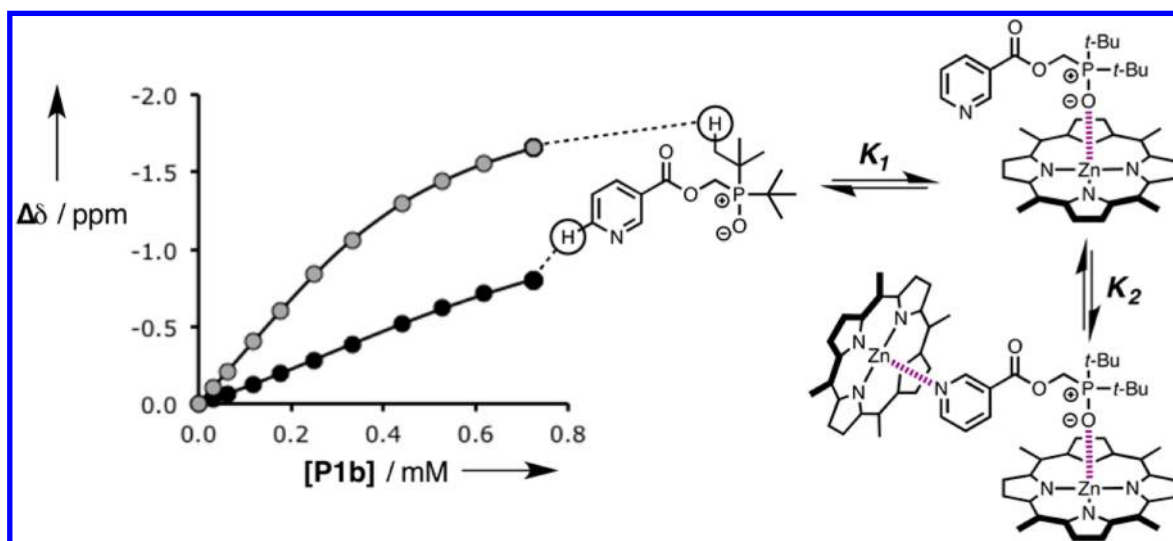


Figure 13. Data from a ^1H NMR titration of **P1b** into **L2g** in toluene- d_8 at 298 K. The changes in chemical shift for the signals due to the *tert*-butyl group (gray) and the pyridine α proton (black) are shown along with the lines of best fit to a 2:1 binding isotherm. The predominant binding modes in the 1:1 and 2:1 complexes are shown.

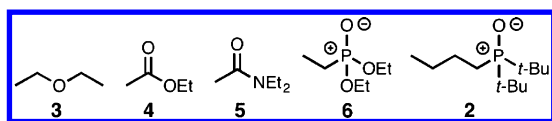


Figure 14. Compounds used to measure $K(\text{O})$ for coordination of H-bond acceptor groups to a zinc porphyrin and K_{ref} for intermolecular H-bonding interactions with *p*-cresol.

Table 7. Association Constants (M^{-1}) for the Formation of Intermolecular H-Bonds Measured by ^1H NMR Titrations at 298 K (K_{ref}) and Estimated Using Equation 3 (K_{calc})

solvent	complex	α	β	α_s	β_s	K_{ref}	K_{calc}
TCE	<i>p</i> -cresol-4	3.8	5.4	2.0	1.3	2 ± 1	2
TCE	<i>p</i> -cresol-5	3.8	8.5	2.0	1.3	22 ± 3	16
TCE	<i>p</i> -cresol-2	3.8	10.2	2.0	1.3	80 ± 10	57
toluene	<i>p</i> -cresol-4	3.8	5.4	1.0	2.2	3 ± 1	3
toluene	<i>p</i> -cresol-5	3.8	8.5	1.0	2.2	86 ± 20	110
toluene	<i>p</i> -cresol-2	3.8	10.2	1.0	2.2	760 ± 30	750

$$K_{\text{obs}} = fK_0 \quad (4)$$

where K_0 is the association constant for formation of only the zinc–nitrogen coordination bond and f is given by eq 5:

$$f = 1 + \sum_i \sigma_i K_i \text{EM}_i + \sum_{i,j} \sigma_{ij} K_i \text{EM}_i K_j \text{EM}_j + \dots + \sigma_{ij\dots N} \prod_i K_i \text{EM}_i \quad (5)$$

in which K_i is the association constant for formation of the i th intermolecular H-bond (i.e., $K_{\text{ref},i}$), EM_i is the effective molarity for formation of the i th intramolecular H-bond, and the constants σ are statistical factors that account for the degeneracies of the different bound states (see the Supporting Information for details of the equations of used for different complexes).

The zinc–nitrogen coordination bonds are not identical in all of the complexes, but differences in K_0 cancel out in the DMC,

Table 8. Effective Molarities (EM, in mM) for Intramolecular Amide–Phenol H-Bonds Measured at 298 K in Toluene^a

	L1e	L2e	L3e	L4e	L5e	L6e
P1a	17	130	140	7	19	51
P2a	16	15	14	5	38	36
P3a	7	33	27	22	85	36
P4a	3	— ^b	— ^b	19	5	8

^aThe average error over the data set was $\pm 50\%$. ^bNo interaction detected.

Table 9. Effective Molarities (EM, in mM) for Intramolecular Amide–Phenol H-Bonds Measured at 298 K in TCE^a

	L1e	L2e	L3e	L4e	L5e	L6e
P1a	12	240	220	10	59	74
P2a	23	21	14	— ^b	49	60
P3a	10	50	54	29	42	64
P4a	— ^b	— ^b	— ^b	29	15	13

^aThe average error over the data set was $\pm 50\%$. ^bNo interaction detected.

allowing the value of $\Delta\Delta G^\circ$ to be related to the values of K_i and EM_i by eq 6,

$$e^{-\Delta\Delta G^\circ/RT} = \frac{f_A f_D}{f_B f_C} \quad (6)$$

where the values of f_A , f_B , f_C , and f_D are given by eq 5.

Solving eqs 5 and 6 for EM_i using the values of $\Delta\Delta G^\circ$ in Tables 1–6 and the values of K_i in Table 7 gave the results reported in Tables 8–11. Values of EM are not reported for the phosphine oxide ligands because of contamination of the DMCs by zinc–oxygen coordination complexes. The values of EM for formation of intramolecular H-bonds in Tables 8–11 span 2 orders of magnitude, ranging from 3 to 240 mM.

Figure 15 compares the values of EM measured in TCE with the corresponding values measured in toluene. There is good agreement between the measurements in these two solvents for

Table 10. Effective Molarities (EM, in mM) for Intramolecular Ester–Phenol H-Bonds Measured at 298 K in Toluene^a

	L1f	L2f	L3f	L4f	L5f	L6f
P1a	— ^b	170	150	— ^b	— ^b	— ^b
P2a	— ^b	— ^b	— ^b	— ^b	— ^b	— ^b
P3a	— ^b	— ^b	38	— ^b	— ^b	— ^b
P4a	— ^b	— ^b	— ^b	— ^b	— ^b	— ^b

^aThe average error over the data set was $\pm 50\%$. ^bNo interaction detected.

Table 11. Effective Molarities (EM, in mM) for Intramolecular Ester–Phenol H-Bonds Measured at 298 K in TCE^a

	L1f	L2f	L3f	L4f	L5f	L6f
P1a	— ^b	230	230	— ^b	— ^b	— ^b
P2a	— ^b	— ^b	— ^b	— ^b	— ^b	— ^b
P3a	— ^b	— ^b	66	— ^b	— ^b	— ^b
P4a	— ^b	— ^b	— ^b	— ^b	— ^b	— ^b

^aThe average error over the data set was $\pm 50\%$. ^bNo interaction detected.

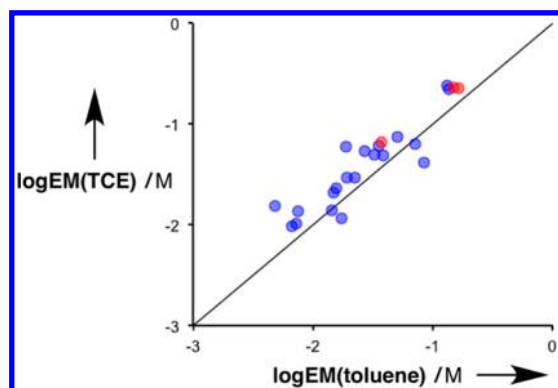


Figure 15. Comparison of effective molarities (EM) for formation of intramolecular H-bonds measured in TCE with the corresponding values measured in toluene. Data for amide (Le) and ester (Lf) ligands are shown in blue and red, respectively. The line corresponds to $\log EM(\text{TCE})/M = \log EM(\text{toluene})/M$.

both the amide and ester ligands. Figure 16 shows that the values of EM measured for ester–phenol H-bonds are practically identical to the corresponding values for amide–phenol H-bonds if we compare ligands that have the H-bond acceptor group located at the same point on the ligand framework. The results for these systems therefore suggest that EM is independent of the solvent and the polarity of the H-bond acceptor.

We can now compare the results for these new ligand systems with the values of EM reported previously for the corresponding phosphonate diester and ether ligand series (La and Ld; see Figures 3 and 5).^{27,28,31,32} Figure 17 compares the values of EM for the phosphonate diester ligands (La) with the corresponding values for the other three ligand families. We previously noted the discrepancy between the values of EM measured for ether and phosphonate diester ligands (Figure 17a).³¹ Although the values of EM fall within the same window (1 mM to 1 M), there is no clear relationship between the phosphonate diester EM values and the corresponding values measured for the other ligand systems. This is particularly

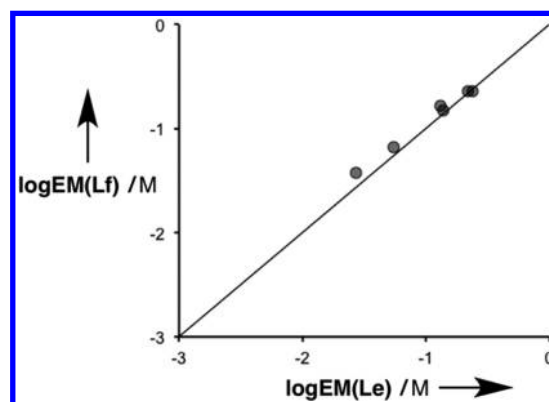


Figure 16. Comparison of effective molarities (EM) for formation of intramolecular ester–phenol H-bonds (Lf) with the corresponding values for amide–phenol H-bonds (Le). The line corresponds to $\log EM(\text{Lf})/M = \log EM(\text{Le})/M$.

striking for the amide ligands (Figure 17b), where there are a large number of data points available for comparison ($r^2 = 0.3$ for 38 data points). Figure 18 compares the values of EM for the ether ligands (Ld) with the corresponding values for the amide and ester ligand families, and here the agreement is much better. The results in Figures 16–18 suggest that although the values of EM are similar for different functional groups, there is sufficient variation in geometry, conformation, and steric bulk to obscure correlations in the value of EM. The more similar the geometry of the functional groups (e.g., esters and amides in Figure 16), the more similar are the values of EM. The EM values for ethers also show a reasonably good correlation with the values for esters and amides, but the phosphonate diesters are sufficiently different in structure to show qualitatively different behavior.

CONCLUSIONS

We previously used porphyrin–pyridine complexes to measure values of EM for intramolecular H-bonding of phenols with phosphonate diesters and ethers in toluene and in TCE.^{27,28,31,32} Although some trends were observed, it was difficult to draw general conclusions from those experiments. In the present work, we expanded the range of H-bond acceptors to include phosphine oxides, amides, and esters. Families of pyridine ligands that place the oxygen H-bond acceptor of these functional groups at the same point on the ligand framework were synthesized. The interactions of these ligands with eight different zinc porphyrins in two solvents (toluene and TCE) were investigated using UV/vis absorption and fluorescence titrations and, in the case of very high association constants ($>10^8 \text{ M}^{-1}$), a competitive ligand displacement experiment. The 288 association constants were used to construct 144 different DMCs to quantify the contributions of intramolecular H-bonds to the overall stabilities of the complexes. In complexes with poor geometric complementarity and weak H-bond acceptors, no H-bonding was detected. However for the most polar H-bond acceptor, phosphine oxide, in the least polar solvent, toluene, intramolecular H-bonding was detected for all 24 different porphyrin–ligand geometries.

¹H NMR spectroscopy showed that a phosphine oxide oxygen binds more strongly than a pyridine nitrogen to a zinc porphyrin, so the complexes used in DMCs for this ligand series had different structures. As a result, the DMC underestimated the contribution of intramolecular phosphine

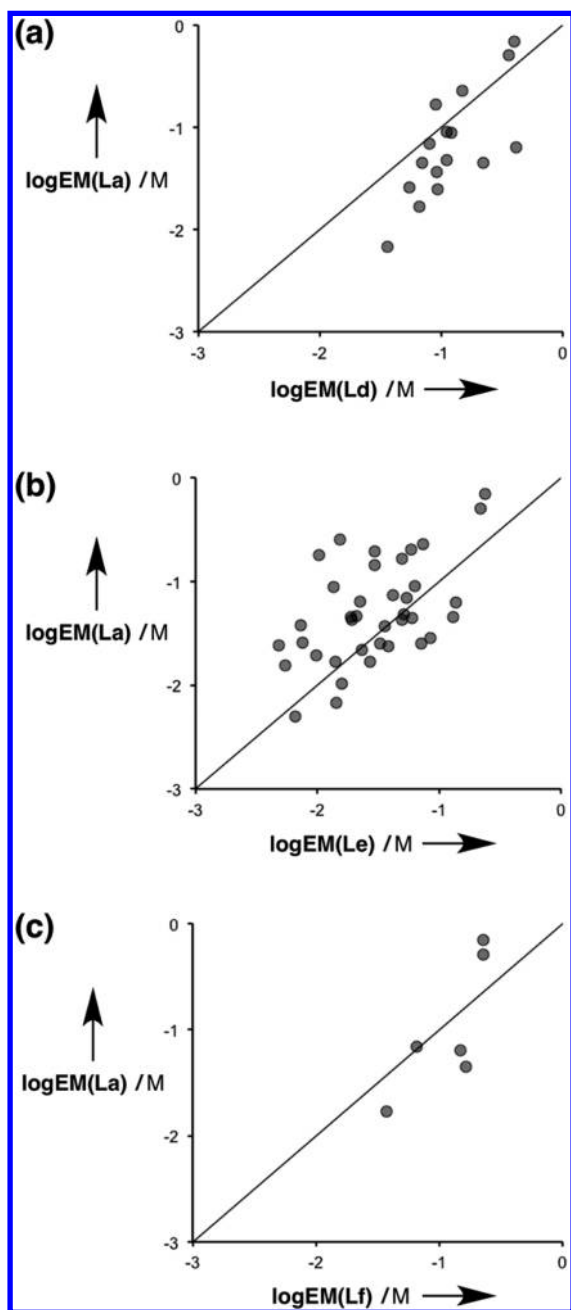


Figure 17. Comparison of effective molarities (EM) for formation of intramolecular phosphonate diester–phenol H-bonds (**La**) with the corresponding values for (a) ether–phenol H-bonds (**Ld**), (b) amide–phenol H-bonds (**Le**), and (c) ester–phenol H-bonds (**Lf**). The line in each panel corresponds to $y = x$.

oxide–phenol H-bonds, and it was not possible to determine accurate values of EM for this ligand series. For the ester and amide ligand series, it was possible to construct reliable DMCs and hence to determine values of EM for the intramolecular H-bonds. The values of EM range from 3 to 240 mM depending on the supramolecular architecture. There is excellent agreement between the values measured in toluene and in TCE as well as between the values measured for amide ligands and the corresponding ester ligands having the oxygen acceptor located at the same site on the ligand framework. When these results are compared with the values of EM obtained previously for different functional groups, the agreement is not so good.

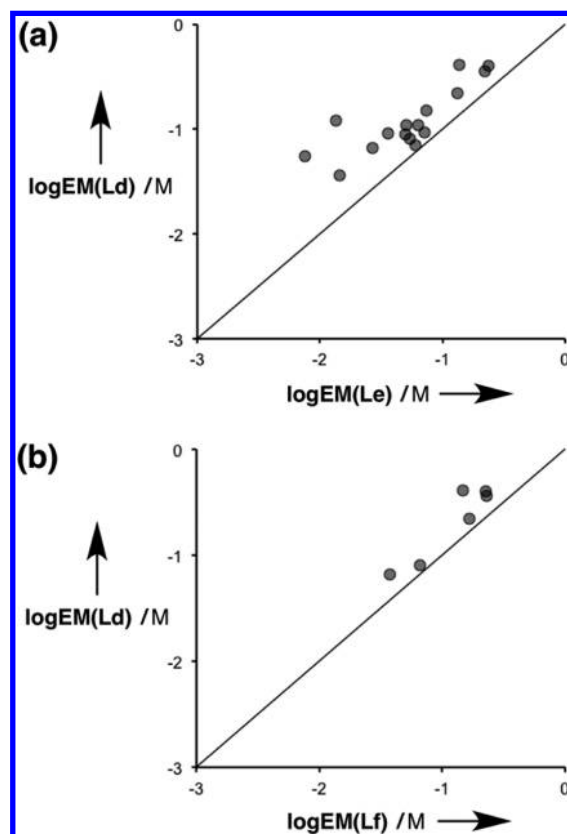


Figure 18. Comparison of effective molarities (EM) for formation of intramolecular ether–phenol H-bonds (**Ld**) with the corresponding values for (a) amide–phenol H-bonds (**Le**) and (b) ester–phenol H-bonds (**Lf**). The line in each panel corresponds to $y = x$.

There is a reasonable correlation with the EM values measured for ether ligands but little correlation with EM values for phosphonate diester ligands. Although the values of EM are qualitatively similar for different functional groups with different H-bonding properties, good quantitative agreement was obtained only for functional groups that have similar geometric and conformational properties (e.g., amides and esters).

In conclusion, we have now collected data on intramolecular H-bonds between phenol and five different H-bond acceptors in 24 different supramolecular architectures and two different solvents. The values of EM fall in the range 1–1000 mM depending on the geometric complementarity of the system, but they do not depend on the solvent or the intrinsic strength of the H-bond (i.e., the polarity of the acceptor group). We previously noted some variations in EM with the nature of the H-bond acceptor, but these differences are now ascribed to differences in conformation. Functional groups with quite different H-bonding properties and very similar geometrical properties, such as amides ($\beta = 8.5$) and esters ($\beta = 5.3$), give very similar values of EM. In contrast, functional groups with similar H-bonding properties and different geometrical properties, such as amides ($\beta = 8.5$) and phosphonate diesters ($\beta = 8.9$), show little correlation in the values of EM. We previously noted that EM varies with solvent for the phosphonate diester ligands but not for the ether ligands. The data reported here show that EM is independent of solvent for both the amide and ester ligand series, so it appears that the phosphonate diester system is anomalous, which may be related to the steric bulk of

this group. The systems for which we have been able to collect the most data are the phosphonate diester and amide ligands. Although the values of EM for these two systems fall in the same window, there is little correlation between the two data sets. The effects of relatively subtle changes in the geometry of the H-bond acceptor group therefore appear to be comparable to the effects of more gross changes in supramolecular architecture.

■ EXPERIMENTAL SECTION

¹H NMR Titrations. NMR titrations were carried out by preparing a 2 mL sample of host at a known concentration (2–20 mM), after which 0.6 mL of this solution was removed and an ¹H NMR spectrum was recorded. A 1 mL solution of guest (25–230 mM) was prepared using the stock host solution to ensure that the concentration of host remained constant throughout the titration. Aliquots of guest solution were added successively to the NMR tube containing the host, and the NMR spectrum was recorded after each addition. Changes in chemical shift were analyzed in Microsoft Excel using the appropriate binding isotherms. Each titration was repeated at least three times, and the experimental error is quoted as twice the standard deviation at a precision of one significant figure.

Automated UV/vis Absorption Titrations. UV/vis titrations were carried out using a BMG FLUOstar Omega plate reader equipped with a UV/vis detector and equilibrated at 298 K. A 5 mL solution of porphyrin at a known concentration (1–5 μM) and a 10 mL solution of ligand at a known concentration (8–40000 μM) were prepared using spectroscopic-grade solvent. A 150 μL aliquot of the porphyrin solution was added to a well of a Hellma quartz microplate, and the absorbance was recorded at five wavelengths. Aliquots of the ligand solution (3, 6, or 10 μL) were successively added to the well, and the absorbance was recorded after each addition. Changes in absorbance were fit to a 1:1 binding isotherm in Microsoft Excel to obtain the association constant. Each titration was repeated at least three times, and the experimental error is quoted as twice the standard deviation at a precision of one significant figure.

Automated Fluorescence Titrations. Fluorescence titrations were carried out using the BMG FLUOstar Omega plate reader equilibrated at 298 K. A 10 mL solution of porphyrin at a known concentration (0.1–1 μM) and a 10 mL solution of ligand at a known concentration (5–63 μM) were prepared using spectroscopic-grade solvent. A 150 μL aliquot of the porphyrin solution was added to each of 12 wells of a Hellma quartz microplate. Different volumes of ligand solution (0–150 μL) were added to each well, and solvent was added to give a total volume of 300 μL. The excitation wavelength was set at 420 or 430 nm, and the fluorescence emission was measured at four wavelengths (590, 600, 620, and 650 nm) for each well. Changes in fluorescence emission were fit to a 1:1 binding isotherm in Microsoft Excel to obtain the association constant. Each titration was repeated at least three times, and the experimental error is quoted as twice the standard deviation at a precision of one significant figure.

Manual Fluorescence Titrations. Fluorescence titrations were carried out using a Hitachi F-4500 fluorescence spectrophotometer at 298 K. A 10 mL solution of porphyrin at a known concentration (0.04–0.05 μM) was prepared in spectroscopic-grade solvent. A 2 mL aliquot of this host solution was loaded into a 1 cm path length fluorescence cuvette, and the fluorescence emission spectrum was recorded from 500 to 750 nm with excitation at 427 nm. A 2 mL solution of ligand (0.1–1 μM) was prepared using the host stock solution to ensure that the concentration of the host remained constant throughout the titration. Aliquots of the ligand solution were added successively to the cuvette, and the emission spectrum was recorded after each addition. Changes in fluorescence emission were fit to a 1:1 binding isotherm in Microsoft Excel to obtain the association constant. Each titration was repeated at least three times, and the experimental error is quoted as twice the standard deviation at a precision of one significant figure.

Fluorescence Displacement Titrations. Fluorescence displacement titrations were carried out using a Hitachi F-4500 fluorescence

spectrophotometer at 298 K. A 20 mL solution of **Q** at known concentration (about 10 mM) was prepared using spectroscopic-grade solvent. A 10 mL solution of porphyrin was prepared at known concentration (about 0.5 μM) by dissolving the porphyrin in the **Q** stock solution. A 2 mL solution of ligand was prepared at a known concentration (about 1 μM) by dissolving the ligand in the porphyrin–**Q** stock solution, to ensure that the concentration of the porphyrin and **Q** remained constant throughout the titration. A 2 mL aliquot of the porphyrin–**Q** stock solution was loaded into a 1 cm path length fluorescence cuvette, and the fluorescence emission spectrum was recorded between 500 and 750 nm with excitation at 427 nm. Aliquots of the ligand solution were added successively to the cuvette, and the emission spectrum was recorded after each addition. An Excel spreadsheet was used to fit the fluorescence emission intensity at fixed wavelengths to a 1:1 binding isotherm with a linear correction to allow for nonspecific effects (e.g., additional weaker binding interactions at secondary sites or additional absorbance due to the ligand at high concentrations). This gave the apparent association constant (K_{app}), which was used to determine the association constant for formation of the porphyrin–ligand complex as explained below. Each titration was repeated at least three times, and the experimental error is quoted as twice the standard deviation at a precision of one significant figure.

Titration data from the displacement experiment could be fit to a simple 1:1 binding isotherm provided that **Q** was present in a large excess relative to the porphyrin and that the total concentration of **Q** was constant throughout the titration. This can be understood as follows. In a simple titration of a porphyrin with a ligand, where **Q** is not present, the concentration of the porphyrin–ligand complex, [PL], is given by eq 7,

$$[PL] = K_L[P][L] \quad (7)$$

where [P] is the concentration of free porphyrin and [L] is the concentration of free ligand. The total concentrations of porphyrin and ligand at any point in the titration, $[P]_T$ and $[L]_T$, are given by eqs 8 and 9:

$$[P]_T = [P] + [PL] \quad (8)$$

$$[L]_T = [L] + [PL] \quad (9)$$

Substituting [P] from eq 8 and [L] from eq 9 into eq 7 and rearranging gives eq 10:

$$[PL] = K_L([P]_T - [PL])([L]_T - [PL]) \quad (10)$$

This is the equation that is solved in fitting titration data to a 1:1 binding isotherm.

Now consider the effect of the presence of another ligand **Q** that competes with L for binding to the porphyrin. Instead of eq 8, the total porphyrin concentration at any point in the titration is now given by eq 11:

$$[P]_T = [P] + [PL] + [PQ] \quad (11)$$

The concentration of the porphyrin–quencher complex, [PQ], is given by eq 12:

$$[PQ] = K_Q[P][Q] \quad (12)$$

where [Q] is the concentration of free quencher ligand. Substituting [PQ] from eq 12 into eq 11 and rearranging gives eq 13.

$$[P] = \frac{1}{1 + K_Q[Q]}([P]_T - [PL]) \quad (13)$$

Substituting [P] from eq 13 and [L] from eq 9 into eq 7 gives eq 14:

$$[PL] = \frac{K_L}{1 + K_Q[Q]}([P]_T - [PL])([L]_T - [PL]) \quad (14)$$

Comparison of eq 14 with eq 10 shows that the only difference introduced by the presence of **Q** is that K_L is replaced by $K_L/(1 + K_Q[Q])$. Thus, the association constant obtained by fitting the displacement titration data to a 1:1 binding isotherm, K_{app} , is related to

K_L by eq 2. The values of K_Q used in eq 2 were determined by UV/vis titrations of **Q** into the relevant porphyrin solutions (Table 12).

Table 12. Association Constants for the Formation of Zinc Porphyrin-Q Complexes (K_Q) Measured by UV/vis Absorption Titrations at 298 K in Toluene

porphyrin	$K_Q/10^4 \text{ M}^{-1}$
P1a	3.3 ± 0.1
P2a	3.1 ± 0.1
P3a	2.3 ± 0.6
P4a	1.6 ± 0.2

■ ASSOCIATED CONTENT

● Supporting Information

Association constants for zinc porphyrin–ligand complexes, NMR study of phosphine oxide ligand binding modes, comparison of the phosphine oxide ligand $\Delta\Delta G^\circ$ values with those for the other ligand series, analysis of the partially bound states for implementation of eqs 4 and 5, and experimental details of ligand synthesis and spectroscopic characterization. This material is available free of charge via the Internet at <http://pubs.acs.org>.

■ AUTHOR INFORMATION

Corresponding Author

c.hunter@sheffield.ac.uk

Notes

The authors declare no competing financial interest.

■ ACKNOWLEDGMENTS

We thank the EPSRC, the China Scholarship Council, and the University of Sheffield for funding.

■ REFERENCES

- (1) Dam, T. K.; Roy, R.; Das, S. K.; Oscarson, S.; Brewer, C. F. *J. Biol. Chem.* **2000**, *275*, 14223.
- (2) Dam, T. K.; Brewer, C. F. *Biochemistry* **2008**, *47*, 8470.
- (3) Badjic, J. D.; Nelson, A.; Cantrill, S. J.; Turnbull, W. B.; Stoddart, J. F. *Acc. Chem. Res.* **2005**, *38*, 723.
- (4) Seel, C.; Vögtle, F. *Angew. Chem., Int. Ed. Engl.* **1992**, *31*, 528.
- (5) Ashton, P. R.; Chrystal, E. J. T.; Glink, P. T.; Menzer, S.; Schiavo, C.; Spencer, N.; Stoddart, J. F.; Tasker, P. A.; White, A. J. P.; Williams, D. J. *Chem.—Eur. J.* **1996**, *2*, 709.
- (6) Izatt, R. M.; Pawlak, K.; Bradshaw, J. S.; Bruening, R. L. *Chem. Rev.* **1991**, *91*, 1721.
- (7) Prins, L. J.; Scrimin, P. *Angew. Chem., Int. Ed.* **2009**, *48*, 2288.
- (8) Hunter, C. A.; Anderson, H. L. *Angew. Chem., Int. Ed.* **2009**, *48*, 7488.
- (9) Ercolani, G.; Schiaffino, L. *Angew. Chem., Int. Ed.* **2011**, *50*, 1762.
- (10) Fasting, C.; Schalley, C. A.; Weber, M.; Seitz, O.; Hecht, S.; Koks, B.; Dornedde, J.; Graf, C.; Knapp, E.-W.; Haag, R. *Angew. Chem., Int. Ed.* **2012**, *51*, 10472.
- (11) Yonetani, T.; Tsuneshige, A. C. R. *Biol.* **2003**, *326*, 523.
- (12) Bellelli, A.; Brunori, M.; Miele, A. E.; Panetta, G.; Vallone, B. *Curr. Protein Pept. Sci.* **2006**, *7*, 17.
- (13) Luque, I.; Leavitt, S. A.; Freire, E. *Annu. Rev. Biophys. Biomol. Struct.* **2002**, *31*, 235.
- (14) Camara-Campos, A.; Hunter, C. A.; Tomas, S. *Proc. Natl. Acad. Sci. U.S.A.* **2006**, *103*, 3034.
- (15) Houk, K. N.; Leach, A. G.; Kim, S. P.; Zhang, X. Y. *Angew. Chem., Int. Ed.* **2003**, *42*, 4872.
- (16) Mammen, M.; Choi, S. K.; Whitesides, G. M. *Angew. Chem., Int. Ed.* **1998**, *37*, 2755.
- (17) Krishnamurthy, V. M.; Semetey, V.; Bracher, P. J.; Shen, N.; Whitesides, G. M. *J. Am. Chem. Soc.* **2007**, *129*, 1312.
- (18) Mulder, A.; Huskens, J.; Reinhoudt, D. N. *Org. Biomol. Chem.* **2004**, *2*, 3409.
- (19) Jiang, W.; Nowosinski, K.; Löw, N. L.; Dzyuba, E. V.; Klautzsch, F.; Schäfer, A.; Huuskonen, J.; Rissanen, K.; Schalley, C. A. *J. Am. Chem. Soc.* **2012**, *134*, 1860.
- (20) Mack, E. T.; Snyder, P. W.; Perez-Castillejos, R.; Bilgic, B.; Moustakas, D. T.; Butte, M. J.; Whitesides, G. M. *J. Am. Chem. Soc.* **2012**, *134*, 333.
- (21) Nelson, D. J.; Ashworth, I. W.; Hillier, I. H.; Kyne, S. H.; Pandian, S.; Parkinson, J. A.; Percy, J. M.; Rinaudo, G.; Vincent, M. A. *Chem.—Eur. J.* **2011**, *17*, 13087.
- (22) Kirby, A. J. *Adv. Phys. Org. Chem.* **1981**, *17*, 183.
- (23) Cacciapaglia, R.; Di Stefano, S.; Mandolini, L. *Acc. Chem. Res.* **2004**, *37*, 113.
- (24) Illuminati, G.; Mandolini, L. *Acc. Chem. Res.* **1981**, *14*, 95.
- (25) Lightstone, F. C.; Bruice, T. C. *Bioorg. Chem.* **1998**, *26*, 193.
- (26) Hogben, H. J.; Sprafke, J. K.; Hoffmann, M.; Pawlicki, M.; Anderson, H. L. *J. Am. Chem. Soc.* **2011**, *133*, 20962.
- (27) Hunter, C. A.; Misuraca, M. C.; Turega, S. M. *J. Am. Chem. Soc.* **2011**, *133*, 582.
- (28) Hunter, C. A.; Misuraca, M. C.; Turega, S. M. *J. Am. Chem. Soc.* **2011**, *133*, 20416.
- (29) Misuraca, M. C.; Grecu, T.; Freixa, Z.; Garavini, V.; Hunter, C. A.; van Leeuwen, P.; Segarra-Maset, M. D.; Turegat, S. M. *J. Org. Chem.* **2011**, *76*, 2723.
- (30) Chekmeneva, E.; Hunter, C. A.; Misuraca, M. C.; Turega, S. M. *Org. Biomol. Chem.* **2012**, *10*, 6022.
- (31) Hunter, C. A.; Misuraca, M. C.; Turega, S. M. *Chem. Sci.* **2012**, *3*, 2462.
- (32) Hunter, C. A.; Misuraca, M. C.; Turega, S. M. *Chem. Sci.* **2012**, *3*, 589.
- (33) Adams, H.; Chekmeneva, E.; Hunter, C. A.; Misuraca, M. C.; Navarro, C.; Turega, S. M. *J. Am. Chem. Soc.* **2013**, *135*, 1853.
- (34) Chekmeneva, E.; Hunter, C. A.; Packer, M. J.; Turega, S. M. *J. Am. Chem. Soc.* **2008**, *130*, 17718.
- (35) Cockcroft, S. L.; Hunter, C. A. *Chem. Soc. Rev.* **2007**, *36*, 172.
- (36) Camara-Campos, A.; Musumeci, D.; Hunter, C. A.; Turega, S. M. *J. Am. Chem. Soc.* **2009**, *131*, 18518.
- (37) Haynes, R. K.; Au-Yeung, T. L.; Chan, W. K.; Lam, W. L.; Li, Z. Y.; Yeung, L. L.; Chan, A. S. C.; Li, P.; Koen, M.; Mitchell, C. R.; Vonwiller, S. C. *Eur. J. Org. Chem.* **2000**, 3205.
- (38) Hunter, C. A.; Sanders, J. K. M.; Beddard, G. S.; Evans, S. J. *Chem. Soc., Chem. Commun.* **1989**, 1765.
- (39) Hunter, C. A. *Angew. Chem., Int. Ed.* **2004**, *43*, 5310.
- (40) Mark, A. E.; van Gunsteren, W. F. *J. Mol. Biol.* **1994**, *240*, 167.